



Large extracellular vesicles secreted by human iPSC-derived MSCs ameliorate tendinopathy *via* regulating macrophage heterogeneity

Teng Ye^{a,b,1}, Zhengsheng Chen^{a,b,1}, Jieyuan Zhang^{b,1}, Lei Luo^{a,c}, Renzhi Gao^{a,b},
Liangzhi Gong^{a,b}, Yuhang Du^d, Zongping Xie^{b,***}, Bizeng Zhao^{b,**}, Qing Li^{a,*}, Yang Wang^a

^a Institute of Microsurgery on Extremities, Shanghai Jiao Tong University Affiliated Sixth People's Hospital, Shanghai, 200233, China

^b Department of Orthopedic Surgery, Shanghai Jiao Tong University Affiliated Sixth People's Hospital, Shanghai, 200233, China

^c School of Biomedical Engineering, Shanghai Jiao Tong University, Shanghai, 200030, China

^d Shanghai EOXOM Biotechnology Co., Ltd, Shanghai, 200210, China

ARTICLE INFO

Keywords:

Large extracellular vesicles
iPSC-derived MSCs
Tendinopathy
Inflammatory regulation
Macrophages

ABSTRACT

Tendinopathy is a common musculoskeletal disorder which results in chronic pain and reduced performance. The therapeutic effect of stem cell derived-small extracellular vesicles (sEVs) for tendinopathy has been validated in recent years. However, whether large extracellular vesicles (IEVs), another subset of extracellular vesicles, possesses the ability for the improvement of tendinopathy remains unknown. Here, we showed that IEVs secreted from iPSC-derived MSCs (iMSC-IEVs) significantly mitigated pain derived from tendinopathy in rats. Immunohistochemical analysis showed that iMSC-IEVs regulated the heterogeneity of infiltrated macrophages and several inflammatory cytokines in rat tendon tissue. Meanwhile, *in vitro* experiments revealed that the M1 pro-inflammatory macrophages were repolarized towards M2 anti-inflammatory macrophages by iMSC-IEVs, and this effect was mediated by regulating p38 MAPK pathway. Moreover, liquid chromatography-tandem mass spectrometry analysis identified 2208 proteins encapsulated in iMSC-IEVs, including 134 new-found proteins beyond current Vesiclepedia database. By bioinformatics and Western blot analyses, we showed that DUSP2 and DUSP3, the negative regulator of p38 phosphorylation, were enriched in iMSC-IEVs and could be transported to macrophages. Further, the immunomodulatory effect of iMSC-IEVs on macrophages was validated in explant tendon tissue from tendinopathy patients. Taken together, our results demonstrate that iMSC-IEVs could reduce inflammation in tendinopathy by regulating macrophage heterogeneity, which is mediated *via* the p38 MAPK pathway by delivery of DUSP2 and DUSP3, and might be a promising candidate for tendinopathy therapy.

1. Introduction

Tendinopathy is a progressive musculoskeletal disorder and is characterized by inflammation and degenerative changes in tendon, which leads to pain, swelling, and impaired performance [1]. However, it is still lack of effective therapeutics currently. Emerging evidence suggests the involvement of inflammation in the occurrence and development of tendinopathy [2,3]. Moreover, researchers have demonstrated that various subtypes of immune cells play a key role in

the inflammatory cascade response during the initiation and progression of tendinopathy and other diseases [4,5]. Among these immunocytes, macrophages are reported to infiltrate the damaged tendon, orchestrate local inflammation, and regulate the healing process [6]. Basically, macrophages manifest a considerable degree of functional variation with diverse phenotypes, including the M1 and M2 phenotypes [7–9]. The M1 macrophages infiltrate to injury sites and release various pro-inflammatory cytokines which are detrimental to tissue repair, such as interleukin-1 (IL-1), tumor necrosis factor- α (TNF- α), and

Peer review under responsibility of KeAi Communications Co., Ltd.

* Corresponding author. Institute of Microsurgery on Extremities, Department of Orthopedic Surgery, Shanghai Jiao Tong University Affiliated Sixth People's Hospital, 600# Yishan Road, Shanghai, 200233, China.

** Corresponding author.

*** Corresponding author.

E-mail addresses: x91034@qq.com (Z. Xie), bz Zhao@sjtu.edu.cn (B. Zhao), liqing_236@aliyun.com (Q. Li).

¹ These authors contributed equally to this work.

<https://doi.org/10.1016/j.bioactmat.2022.08.007>

Received 7 April 2022; Received in revised form 19 July 2022; Accepted 8 August 2022

2452-199X/© 2022 The Authors. Publishing services by Elsevier B.V. on behalf of KeAi Communications Co. Ltd. This is an open access article under the CC BY-NC-ND license (<http://creativecommons.org/licenses/by-nc-nd/4.0/>).

interleukin-6 (IL-6) [10], while the M2 macrophages appear to be involved in the later healing process, which possess the capacity to eliminate intracellular pathogens and promote tendon regeneration [8, 11]. Given the unique property of macrophages, regulating the heterogeneity of macrophages might be a promising therapeutic avenue for the treatment of tendinopathy.

Extracellular vesicles (EVs) are known to be secreted by most cells and encapsulate a variety of nucleic acids, lipids, and proteins from the parental cell [12,13]. In accordance with MISEV 2018 guideline, EVs can be divided into small EVs (sEVs, < 200 nm, pelleted at 100,000 g) and large EVs (lEVs, > 200 nm, pelleted at 10,000 g) by the particle size [14]. In recent years, the therapeutic functions of stem cell-derived sEVs have been widely explored in various diseases including tendinopathy. Several studies have demonstrated the underlying mechanism of sEVs for treating tendinopathy, including modulating tendon inflammation, promoting angiogenesis and balancing the metastasis of tendon extracellular matrix [15,16]. Recently, several studies focusing on the lEVs derived from adult stem cells have revealed that lEVs might achieve similar therapeutic functions as sEVs. For instance, Wu et al. reported that lEVs derived from human Wharton's Jelly mesenchymal stem cells (MSCs) mitigated renal ischemia-reperfusion injury in rats [17]. Lei et al. demonstrated that lEVs secreted from neonatal umbilical cord MSCs rejuvenated aged bone marrow-derived MSCs and slow age-related systematic degeneration [18]. However, whether stem cell-derived lEVs are effective for tendinopathy and the underlying mechanism remains unknown.

In this study, we investigated the therapeutic effect of lEVs secreted from induced pluripotent stem cell-derived MSCs (iMSC-lEVs) in tendinopathy (both in a rat tendinopathy model and an *ex vivo* human pathological tendon tissue culture system) and the regulatory role of iMSC-lEVs on macrophage polarization *in vitro*. Firstly, we isolated both sEVs and lEVs from the culture medium of iMSCs, while the sEVs treatment was regarded as a control. The application of iMSC-lEVs significantly ameliorated the tendinopathy-related pain and regulating the phenotypes of macrophages as well as inflammatory cytokines infiltrated to the pathological tendon tissue in a rat tendinopathy model. Additionally, several *in vitro* experiments including RT-qPCR, flow cytometry analysis, immunofluorescent staining and ELISA showed that iMSC-lEVs could repolarize the macrophages from M1 phenotype towards M2 phenotype. Next, we verified this effect of iMSC-lEVs on macrophage was mediated by regulating p38 MAPK signaling pathway. To identify the upstream proteins encapsulated in iMSC-lEVs, liquid chromatography coupled with tandem mass spectrometry (LC-MS/MS) was further performed and discovered a variety of 2208 proteins. Through bioinformatic analysis, we revealed that iMSC-lEVs regulated the p38 MAPK signaling pathway by transferring DUSP2 and DUSP3. Collectively, we show for the first time that iMSC-lEVs are effective in tendinopathy, which alleviate the inflammation by the regulation of macrophage heterogeneity, suggesting iMSC-lEVs as a promising therapeutic candidate for inflammatory diseases.

2. Materials and methods

2.1. Derivation and culture of iPSC-derived MSCs

A human induced pluripotent stem cell line (iPS-S-01) was kindly provided by the Institute of Biochemistry and Cell Biology of the Chinese Academy of Sciences in agreement with Liao and Xiao [19]. hiPSC-MSCs (iMSCs) were generated according to our previous report [20]. iMSCs were cultured in the serum-free ncMission hMSC Medium (RP02010, Nuwacell Biotechnologies, China) and the culture medium was replaced and collected every two days. iMSCs were passaged when the cell confluency reached to about 80%. Passage 5 to 10 of iMSCs were used for the following experiments.

2.2. Isolation of iMSC-derived large EVs (lEVs) and small EVs (sEVs)

iMSC-derived lEVs and sEVs were isolated by serial centrifugation with ultracentrifugation according to previous described methods [14, 21]. Briefly, the iMSC culture medium was collected and centrifuged at 300×g (4 °C) for 10 min to remove dead cells. Then, the supernatant was centrifuged at 2000×g (4 °C) for 20 min to remove apoptotic bodies and cell debris. Next, the supernatant was centrifuged at 10,000×g (4 °C) for 30 min to pellet the lEVs. Afterwards, the lEVs-depleted supernatant was filtered through a 0.22 μm disposable membrane (Millipore, US), and further ultracentrifuged at 100,000×g (4 °C) for 70 min using an SW 32 Ti Rotor Swinging Bucket rotor (Beckman Coulter, Fullerton, CA) to pellet the sEVs. The lEVs pellet was re-suspended in a large volume of PBS followed by 10,000×g (4 °C) centrifugation for 30 min to wash the sample. Likewise, the sEVs pellet was re-suspended in a large volume of PBS followed by 100,000×g (4 °C) ultracentrifugation for 70 min to wash the sample. After PBS-washing, the lEVs and sEVs were respectively re-suspended in sterile PBS and stored at −80 °C for up to 1 month before use.

2.3. Transmission electron microscopy (TEM)

For TEM observation, a total of 10 μL lEVs or sEVs suspensions were dropped onto a formvar-carbon-coated grid (400 meshes) and dried for 20 min. Then, the grids were rinsed with PBS and fixed in 1% glutaraldehyde for 5 min, which were further rinsed with deionized water and stained with uranyl oxalate for 5 min. After drying, the microstructure of lEVs or sEVs were imaged by TEM (Hitachi H-7650, Tokyo, Japan).

2.4. Size distribution and particle concentration

The size distribution and particle concentration of sEVs and lEVs were measured by nanoparticle tracking analysis (NTA) using the ZetaView instrument (Particle Metrix, Germany). Samples were diluted in PBS at proper ratios and then administered under controlled flow. The size distribution and particle concentration data were given by the ZetaView Software 8.03.04.01 (Particle Metrix, Germany).

2.5. Protein concentration assay

The protein concentration of lEVs and sEVs were quantified using Pierce BCA Protein Assay Kit (Cat#23225, Thermo Fisher Scientific, USA) according to the instruction manual. In brief, lEVs and sEVs were lysed with RIPA lysis buffer (Beyotime, Jiangsu, China) and the proteins were harvested following the manual. Next, a total of 10 μL protein sample was loaded into each well of a 96-well-plate and 200 μL of the working reagent was added. Subsequently, the plate was incubated for 30 min at 37 °C and the absorbance was measured at 562 nm. The standard curve was used to determine the protein concentration of lEVs and sEVs sample.

2.6. Animal model and experimental design

All animal experimental procedures were approved by the Animal Research Committee of Shanghai Jiao Tong University Affiliated Sixth People's Hospital (SYXK2021-0028, Shanghai, China). A total of thirty adult male Sprague Dawley rats (200–300 g) underwent sham surgery or tendinopathy-modeling surgery were randomly and averagely divided into four groups [1]: Sham group [2]; Model + PBS group [3]; Model + sEVs group [4]; Model + lEVs group. The rat tendinopathy model was established by a single injection of carrageenan solution according to previous studies [22–25]. Briefly, we dissolved carrageenan powder (Sigma-Aldrich/Merck KGaA, Germany) with sterile PBS to obtain a 4% carrageenan solution. For the model group, rats were anesthetized with isoflurane, positioned supine, and the fur above the right quadriceps was shaved. Then, 100 μL of the 4% carrageenan solution was injected

around the right quadriceps tendon with a 27-gauge needle under the guidance of ultrasound imaging (Fujifilm VisualSonics; Bothell, Washington, USA). The potential direct tendon injury by the syringe needle was carefully avoided. For the sham group, rats were injected with 100 μL PBS around the right quadriceps tendon under ultrasonic guidance. Subsequently, to investigate the therapeutic effect of sEVs and IEVs, 100 μL of PBS, sEVs (1×10^9 particles) or IEVs (1×10^8 particles) were injected around the quadriceps tendon under ultrasonic guidance one week after carrageenan injection and once per week for four weeks in total. All rats were housed under specific-pathogen-free conditions, 12/12-h light/dark cycle, and were allowed free access to food and water. At two and four weeks after treatment, the right quadriceps tendons were harvested for following histological evaluation after a lethal overdose of anesthetic.

2.7. Assessment of pain-related behaviors in tendinopathy rats

Pain is the most frequent complaint in patients with tendinopathy. The pain-related behaviors (below) in each group were assessed one week after carrageenan injection and once per week for five weeks in total.

2.7.1. Hind-paw withdrawal threshold

Reflexive measures of pain using stimulus-evoked responses, such as hind-paw withdrawal threshold, are commonly used to assess tendinopathy-related pain [26]. Hind-paw withdrawal threshold analysis was performed based on our previous report [27]. Briefly, the rats were placed individually in an elevated metal grid cage with sufficient space for them to move their paws while the rest of their body was restricted with plastic plates. After the rats acclimated to the apparatus, the rat's right hind-paw withdrawal threshold (PWT) was assessed by an electronic von Frey instrument (model BIO-EVF4; Bioseb, Vitrolles France). The probe tip of the instrument was gently placed perpendicularly into the mid-plantar surface of the paw, and steadily increasing pressure (between 0 and 150 g) was applied until the hind paw was first lifted. The PWT was recorded as the required pressure to first lift the paw. The data were expressed as PWT in grams (g). Lower PWT values (g) were taken as indicators of pain.

2.7.2. Static weight-bearing

The static weight-bearing (SWB) distribution over the right and left knee was assessed by measuring postural equilibrium between the injected and non-injected leg [26]. Briefly, a rat was placed in the chamber of a weight-bearing measuring device (model #BIO--SWB-TOUCH-M; Bioseb) and allowed to acclimate before regular testing. The force applied through each hind limb to the paw resting on the floor of the chamber was measured in grams (g), and an SWB ratio was calculated as follows:

$$\text{SWB ratio} = \frac{\text{Force applied to right limb}}{\text{Force applied to right limb} + \text{Force applied to left limb}}$$

As the right side received the carrageenan injection, SWB ratios can vary between 0 and 1, with values closer to zero indicating that postural equilibrium favors the rat's left non-injected side. For each rat, the test was given three times at each assessment period, and the mean value was taken as the SWB at that time point.

2.7.3. Gait analysis

Dynamic pain-related gait analysis were measured using the CatWalk system, which objectively quantified behavioral gait adaptation, automatically documenting paw placements on a surface and related parameters of inter-limb coordination [28]. Briefly, rats were placed on an illuminated glass walkway (70 cm long by 8 cm wide) apparatus (Shanghai Mobicell Information Technology, Shanghai, China). A camera below the walkway captures and digitally records footprint

images. These paw print placements and gait parameters (such as print area, swing speed, and duty cycle) were collected and further analyzed by a WalkAnalysator Software (Shanghai Mobicell Information Technology, Shanghai, China). The CatWalk gait test was administered at weeks 5 after carrageenan injection in each group. Print area, swing speed and duty cycle were analyzed by the WalkAnalysator Software and further calculated as Right Hind Limb/Left Hind Limb.

2.8. Histological evaluation and immunohistochemistry

The rat quadriceps tendons in all groups were fixed with 4% PFA for 24 h and then dehydrated with a graded-ethanol series. The dehydrated samples were embedded in paraffin and sectioned at 5 μm thickness parallel to the long axis of tendon. The Hematoxylin-Eosin (HE) Staining Kit (Solarbio, Beijing, China) was used to evaluate the tendon morphology in each group. According to the previously reported Bonar scoring system, the abnormalities of tendons in all groups was assessed [29]. For the immunohistochemistry analysis, tendon sections in each group were deparaffinized in xylene, hydrated through ethanol series and then repaired by using pepsin antigen repair solution. Subsequently, all the sections were blocked with 5% BSA for 30 min and incubated with primary antibodies against CD86 (1:100; 13395-1-AP, Proteintech), CD206 (1:200; ab64693, Abcam), IL-1 β (1:100; ab9722, Abcam), TNF α (1:100; ab220210, Abcam), IL-6 (1:100; ab9324, Abcam), NGF (1:100; ab52918, Abcam). Next, each section was incubated with the HRP-labeled secondary antibodies and DAB (Servicebio, Wuhan, China) was used as HRP-specific substrate. Images were captured using Leica DM6B (Leica Microsystems, Milan, Italy) and further processed with ImageJ software. The positive rate (%) of markers mentioned above in each group was calculated.

2.9. Acquisition of human iliopsoas tendons and tendon tissue culture in vitro

Tendon samples were obtained from 3 female and 1 male patients aged 50 to 80 years-old from the surgery of iliopsoas tenotomy during hip arthroscopy. Tendon sample from each patient was separated into 2 pieces (about $3 \times 3 \times 3 \text{ mm}^3$ for each piece) and respectively incubated with 2 mL complete medium with or without iMSC-IEVs for 72 h in 12-well culture plates. After the incubation, tendon samples were routinely processed, embedded sectioned and incubated overnight with CD86 (1:100; 13395-1-AP, Proteintech), CD206 (1:200; ab64693, Abcam), IL-1 β (1:100; ab9722, Abcam), TNF α (1:100; ab220210, Abcam), IL-6 (1:100; ab9324, Abcam), and NGF (1:100; ab52918, Abcam). Further, the sections were incubated with HRP-labeled secondary antibodies. Ethics approval was obtained from the Shanghai Sixth People's Hospital Ethics Committee (Approval code: 2022-KY-084(K)).

2.10. Culture and experimental protocol of RAW 264.7 cells

Murine macrophage RAW 264.7 cells were purchased from the Cell Bank of the Chinese Academy of Sciences (Shanghai, China) and cultured in Dulbecco's Modified Eagle's Medium (DMEM, Corning) supplemented with 10% fetal bovine serum (FBS, Gibco). The cell culture was maintained at 37 $^{\circ}\text{C}$ in 5% CO_2 and 95% humidity.

Raw 264.7 cells were treated with 100 ng/mL lipopolysaccharide (LPS, Cat#L6529, Sigma-Aldrich) for 6 h to induce the M1 phenotype and the culture medium was replaced. After the M1 phenotype induction, RAW 264.7 cells were further incubated with fresh medium containing iMSC-sEVs (10^9 particles/mL), iMSC-IEVs (10^8 particles/mL) or vehicle (PBS) for an additional 48 h. RAW 264.7 cells without LPS and sEVs/IEVs treatments were regarded as M0 phenotype negative control. After 48 h incubation, the RAW 264.7 cells were collected for further RNA isolation, flow cytometer analysis or immunofluorescence staining, while the supernatants were collected for enzyme-linked immunosorbent assay.

2.11. Uptake of iMSC-sEVs/IEVs *in vivo* and *in vitro*

To determine the retention of sEVs or IEVs around quadriceps tendon *in vivo*, sEVs or IEVs were stained with DiR fluorescent dye (Thermo Fisher, USA) according to previous report [30]. Briefly, sEVs or IEVs were incubated with DiR for 15 min under room temperature and followed by 100,000 g ultracentrifugation in PBS to remove the unlabeled DiR dye. 100 μ L DiR-labeled sEVs (10^9 particles in 100 μ L PBS) or IEVs (10^8 particle in 100 μ L PBS) were injected to the right quadriceps of rats with a single dose. The rats were anesthetized and the DiR fluorescent signals were detected by an IVIS Spectrum imaging system (PerkinElmer, USA) at 2, 24, 48 h after injection. The quadriceps tendons at 24 h after injection were harvested and incubated with the primary antibody against CD68 (1:100, ab283654, Abcam), Scleraxis (1:100, sc-518082, Santa Cruz), CD146 (1:100, ab75749, Abcam) overnight and followed by second antibody and DAPI staining.

In the RAW 264.7 cells *in vitro* experiment, sEVs or IEVs were stained with DiI fluorochrome (Thermo Fisher, USA) for the same incubation and washing procedures mentioned above. Then, DiI-labeled sEVs/IEVs were added into culture medium and incubated with RAW 264.7 cells (LPS-stimulated) for 6 h at 37 °C or 4 °C. Next, culture medium was discarded, the cell cytoskeleton was stained with FITC-labeled phalloidin (C1033, Beyotime) and the cell nuclei were stained with DAPI (2 μ M, Sigma) prior to the image capture using the fluorescence microscope (Leica, DM6B, Germany).

2.12. Real-time quantitative polymerase chain reaction (RT-qPCR) analysis

To evaluate the expression of target genes in RAW 264.7 cells, total RNA was extracted using QIAzol Lysis Reagent and RNeasy Mini Columns (Qiagen, Valencia, CA) according to the manufacturer's instructions. The concentration and purity of the total RNA were confirmed using a NanoDrop Spectrophotometer (ThermoFisher Scientific). The RevertAid First Strand cDNA Synthesis Kit (Thermo Scientific, CA; Cat#K1622) was applied to perform the Reverse transcriptase. Subsequently, RT-qPCR was performed using the ABI Prism 7900HT Real Time System (Applied Biosystems, CA) with SYBR green kit (Roche Applied Science; Cat# 04913850001). The sequences of the primers in this study are listed in [Supplemental Table 1](#).

2.13. Flow cytometry analysis

For the identification of iMSC surface markers, single-cell suspension was collected and the cell number was counted using a hemocytometer. Next, iMSCs were incubated with 1% bovine serum albumin (BSA, Gibco) to block non-specific antigens. Then, 10^6 iMSCs were incubated with following conjugated monoclonal antibodies at 4 °C for 30 min: CD29-PE (1:100; 561795, BD Biosciences), CD44-FITC (1: 100; 560977, BD Biosciences), CD73-PE (1: 100; 561014, BD Biosciences), CD90-PE (1:100; 328109, Biologend), CD105-FITC (1:100; 561443, BD Biosciences), CD146-PE (1:100; 561013, BD Biosciences), CD34-APC (1: 100; 560940, BD Biosciences), CD45-FITC (1:100; 560976, BD Biosciences), CD133-PE (1: 100; 130-080-801, Miltenyi Biotec), and HLA-DR-PE (1:100; 560943, BD Biosciences). The uncombined antibodies were then washed twice with 1% BSA. The cells were resuspended in 400 μ L 1% BSA and further analyzed using CytoFLEX flow cytometer (Beckman Coulter Life Science, USA). Data were processed by FlowJo Software (TreeStar, Ashland, OR).

For the flow cytometry analysis of RAW 264.7 cells, single cells were collected and re-suspended into suspension. After blocking non-specific antigens as mentioned above, 10^6 RAW 264.7 cells were incubated with antibody CD86-PE (1:100; 561963, BD Biosciences) at 4 °C for 30 min. For intracellular staining, cells were permeabilized and fixed with the intracellular staining kit (00-5523-00, eBioscience) and then washed and stained with antibody CD206-APC (1:100; 565250, BD Biosciences).

The stained cells were resuspended and analyzed using CytoFLEX flow cytometer as described above. Data were processed by FlowJo Software (TreeStar, Ashland, OR).

2.14. Immunofluorescence staining

For cultured RAW 264.7 cell preparation, cells were rinsed with sterile PBS and fixed with PFA for 20 min at room temperature. Next, cells were permeabilized with 0.1% Triton X-100 for 15 min at room temperature, followed by a blocking step with 5% (w/v) BSA for 1 h at room temperature. Then, cells were incubated at 4 °C overnight with the following primary antibodies against CD86 (1:100; 14-0862-81, eBioscience) and CD206 (1:200; AF2535, R&D Systems). After overnight incubation, secondary antibodies (1:500; Invitrogen) were applied and followed by DAPI staining. Images were obtained using a Leica DM6B (Leica Microsystems, Milan, Italy) and further processed with ImageJ software.

2.15. Enzyme-linked immunosorbent assay (ELISA)

To evaluate the levels of IL-1 β , TNF- α , IL-6, IL-10, TGF- β in the supernatants from RAW 264.7 cells, ELISA analysis was performed. Briefly, following 48 h treatment of PBS, sEVs or IEVs as described above, the culture medium was collected for detecting the concentrations of IL-1 β , TNF- α , IL-6, IL-10, TGF- β using a mouse ELISA kit (Shanghai Westang Bio-Tech Co., LTD., Shanghai, China) according to the manufacturer's instructions. A microplate reader (Thermo Fisher Scientific, Waltham, MA, USA) was applied to measure the absorbance at 450 nm.

2.16. Western blot analysis

For the identification of IEVs and sEVs using Western blot analysis, three positive markers including CD9, CD63, and TSG101, as well as one negative marker GM130, were detected. The protein samples of IEVs and sEVs were collected using RIPA lysis buffer (Beyotime, Jiangsu, China). The Western blot analysis were performed as previously described [27]. Briefly, protein extracts were resolved by SDS-PAGE gels (10 μ g protein/lane) and probed with the indicated antibodies. The following antibodies were used for Western blot analysis: CD63 (1:1000; ab134045, Abcam), CD9 (1: 2000; ab92726, Abcam), TSG101 (1: 1000; sc-7964, Santa cruz), GM130 (1: 1000; ab52649, Abcam). Anti-rabbit IgG or anti-mouse IgG, horseradish peroxidase (HRP)-linked antibody (1:2000; Cell Signaling Technology) was used as secondary antibody and chemiluminescent signals were visualized by the ECL Western Blot detection kit and Bio-RAD imaging system (Bio-RAD, CA, USA).

For the Western analysis of RAW 264.7 cells in the *in vitro* experiment, cells were seeded on a 6-well plate followed by 6 h 100 ng/mL lipopolysaccharide (LPS) stimulation and iMSC-IEVs treatment with or without U-46619. Control cells were cultured with the same time as other groups, but without any treatment. After that, the protein samples of RAW 264.7 cells were collected using RIPA lysis buffer (Beyotime, Jiangsu, China) and quantified using Pierce BCA Protein Assay Kit (Cat#23225, Thermo Fisher Scientific, USA). Total amount of 10- μ g protein of cell lysates were run on SDS-PAGE gels and probed with following primary antibodies: Anti-p38 MAPK (1:1000; 8690 T, Cell Signaling Technology), Anti-p-p38 MAPK (1:1000; 4511 T, Cell Signaling Technology), Anti- β -actin (1:1000; ab133626, Abcam), Anti-DUSP2 (1:500; 27327-1-AP, Proteintech), Anti-DUSP3 (1:50000; ab125077, Abcam), Anti-DUSP2 (1:500; sc-32776, Santa Cruz), Anti-DUSP3 (1:1000; SAB4301843, Sigma-Aldrich). HRP-linked antibody (1:2000; Cell Signaling Technology) was used as secondary antibody and the immunoreactive bands were visualized by the ECL Western Blot detection kit and Bio-RAD imaging system. Furthermore, Anti-DUSP2 (1:500; 27327-1-AP, Proteintech) and Anti-DUSP3 (1:50000; ab125077, Abcam) were used to evaluate DUSP2 and DUSP3 level in

iMSCs and iMSC-IEVs by Western blot analysis as described above.

2.17. RNA-sequencing (RNA-seq) analysis

The RNA-seq analysis was conducted by Shanghai Biotechnology Corporation (Shanghai, China). Briefly, total RNA of RAW 264.7 cells were extracted by RNeasy mini kit (Qiagen, Germany). Next, the TruSeq™ RNA Sample Preparation Kit (Illumina, USA) was adopted to synthesize paired-end libraries according to the TruSeq™ RNA Sample Preparation Guide. The Poly-T oligo-attached magnetic beads were used to purify poly-A containing mRNA molecules. After purification, the mRNA was fragmented into small pieces using divalent cations under 94 °C for 8 min. Reverse transcriptase and primers were adopted to copy RNA fragments into first-strand cDNA and followed by the synthesis of second-strand cDNA via DNA polymerase I and RNase H. Next, these cDNA passed an ending repair procedure and then purified and enriched by PCR to generate the cDNA library. The purified libraries were quantified by Qubit® 2.0 Fluorometer (Thermo Scientific, USA) and confirmed by Agilent 2100 bioanalyzer (Agilent Technologies, USA). Cluster was generated by cBot with the library diluted to 10 pM and then were sequenced on the Illumina HiSeq (Illumina, USA).

2.18. Proteomic analysis

The procedure of iMSC-IEVs proteomic analysis was in consistent with our previous study [31] and performed by the Shanghai Applied Protein Technology Company (Shanghai, China).

2.18.1. Protein isolation and identification

The isolated iMSC-IEVs (400 μ L, obtained from 240 ml of conditioned media) were digested in SDT lysis buffer (4% SDS, 100 mM Tris-

HCl, 1 mM DTT, pH7.6). The lysate was sonicated for 15 min and then heated to 95 °C for 15 min. After centrifuged at 14000 \times g for 40 min, the supernatant was quantified with the BCA Protein Assay Kit (Bio-Rad, USA). 20 μ g of proteins for each sample were mixed with 5 \times loading buffer, respectively, and boiled for 5 min. The proteins were separated on 12.5% SDS-PAGE gel (constant current 14 mA, 90 min).

2.18.2. Filter-aided sample preparation (FASP)

100 μ g of proteins for each sample were incorporated into 30 μ L SDT buffer (4% SDS, 100 mM DTT, 150 mM Tris-HCl pH 8.0). The detergent, DTT and other low-molecular-weight components were removed using UA buffer (8 M Urea, 150 mM Tris-HCl pH 8.0) by repeated ultrafiltration (Microcon units, 10 kD). Then, 100 μ L iodoacetamide (100 mM IAA in UA buffer) was added to block reduced cysteine residues and the samples were incubated for 30 min in darkness. The filters were washed with 100 μ L UA buffer three times and then 100 μ L 25 mM NH_4HCO_3 buffer twice. Finally, the protein suspensions were digested with 4 μ g trypsin (Promega) in 40 μ L 25 mM NH_4HCO_3 buffer overnight at 37 °C, and the resulting peptides were collected as a filtrate. The peptides of each sample were desalted on C18 Cartridges (Empore™ SPE Cartridges C18 (standard density), bed I.D. 7 mm, volume 3 mL, Sigma), concentrated by vacuum centrifugation and reconstituted in 40 μ L of 0.1% (v/v) formic acid. The peptide content was estimated by UV light spectral density at 280 nm using an extinction coefficient of 1.1 of 0.1% (g/l) solution.

2.18.3. Peptide fractionation with high pH reversed-phased

To increase the depth of protein identification, peptide fractionation was performed using Pierce High pH Reversed-Phased Peptide Fractionation kit (Thermo Scientific, 84868). Digest samples were fractionated into five fractions (F1–F5) by an increasing acetonitrile step-

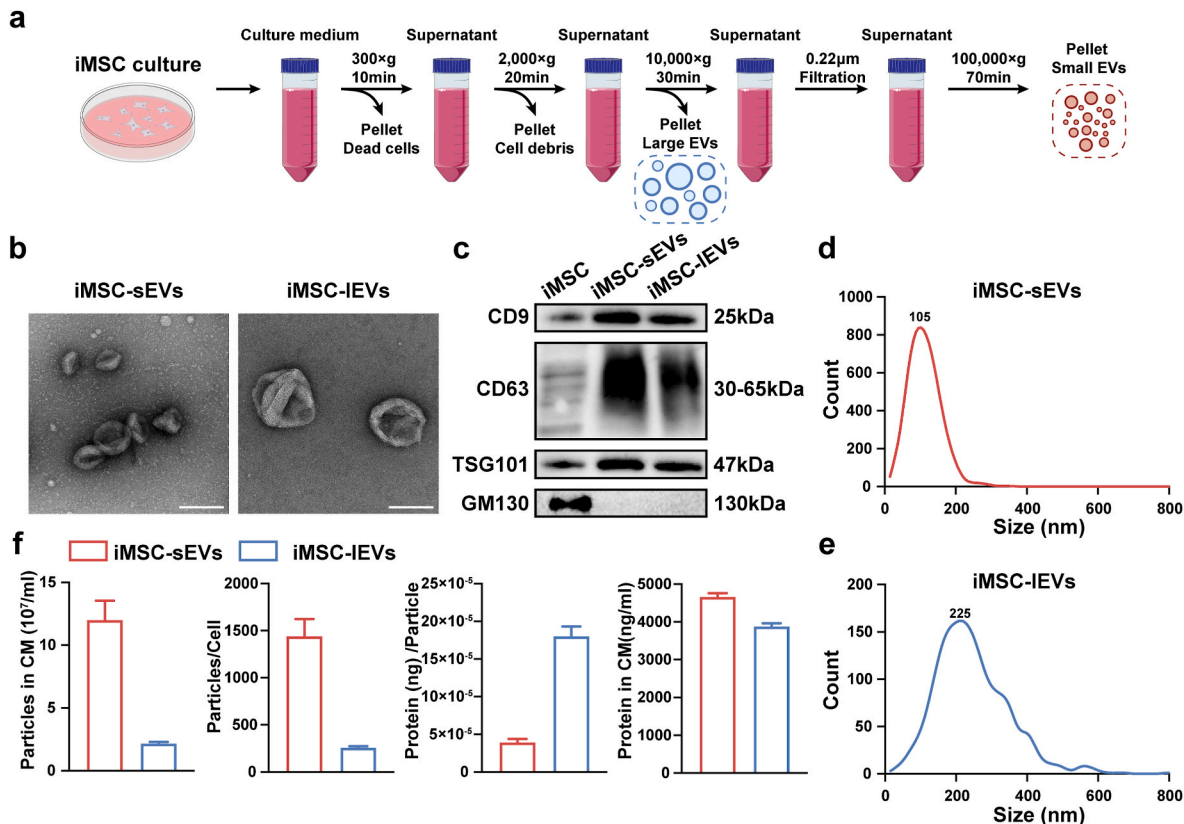


Fig. 1. Characterization of iMSC-sEVs and iMSC-IEVs. (a) Schematic illustration of iMSC-sEVs/IEVs isolation using differential centrifugation. (b) Representative images of iMSC-sEVs/IEVs by TEM, scale bar: 200 nm. (c) Western blot analysis of CD9, CD63, TSG101, and GM130 markers. (d–e) Size distribution of iMSC-sEVs/IEVs. (f) Quantification of iMSC-sEVs/IEVs parameters, including the particle concentration and the protein concentration.

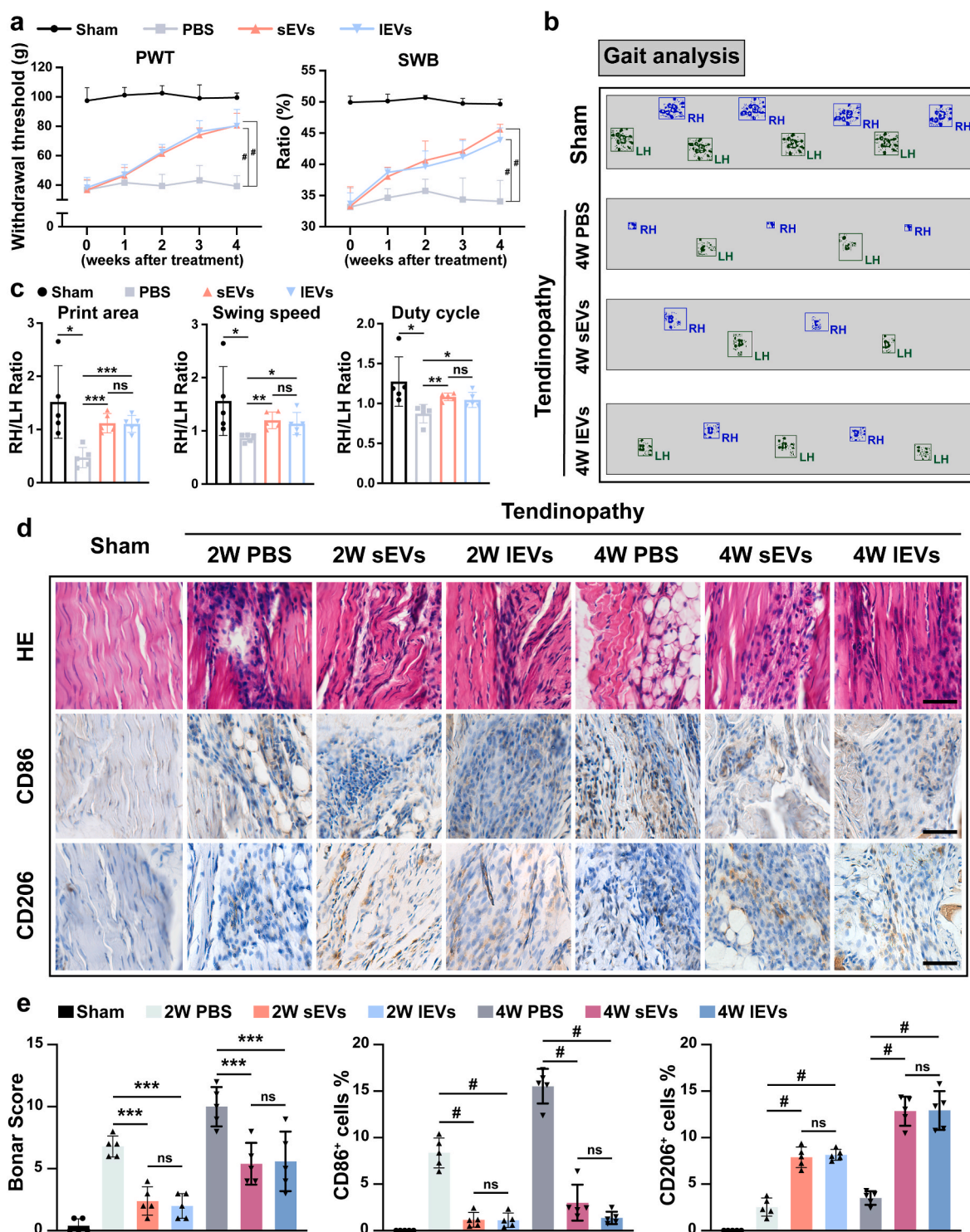


Fig. 2. iMSC-IEVs treatment improved pain-related behaviors and regulated macrophage infiltration *in vivo*. (a) Pain-related behaviors measured by PWT and SWB analysis once per week and up to 4 weeks after treatment in each group (n = 5/group). PWT = hind-paw withdrawal threshold, SWB = static weight-bearing. (b) Representative images of gait analysis indicating the dynamic pain-related behaviors at 4 weeks after treatment in each group. Blue paw prints indicating the right hind and green paw prints indicating the left hind. RH = right hind, LH = left hind. (c) Quantitative analysis of gait analysis including print area, swing speed and duty cycle in each group (n = 5/group). (d) Representative images of HE staining and immunohistochemistry analysis for CD86 and CD206 expression in quadriceps tendon after 2 and 4 weeks treatment with PBS, sEVs or IEVs, as well as sham group. Scale bar: 100 μ m. (e) Semiquantitative histological analysis (Bonar scoring system) and quantitative analysis of immunohistochemical staining for CD86 and CD206 expression (n = 5/group). * $P < 0.05$, ** $P < 0.01$, *** $P < 0.001$, # $P < 0.0001$, ns, nonsignificant difference.

gradient elution according to the kit instructions.

2.18.4. MS data acquisition

The MS analysis were performed using an Easy-nLC 1000 nano-UPLC chromatography (Thermo Scientific) interfaced with a Q-Exactive Orbitrap mass spectrometer (Thermo Scientific) with a nano-electrospray ion source. The sample was loaded onto an Acclaim Pep-Map100 C18 reverse-phase trap column (100 $\mu\text{m} \times 2\text{ cm}$) with nano-Viper fittings (Thermo Scientific) connected to the C18-reversed-phase analytical column (Thermo Scientific Easy Column, 10 cm long, 75 μm inner diameter, 3 μm resin) in buffer A (0.1% Formic acid) and separated with a linear gradient of buffer B (84% acetonitrile and 0.1% formic acid) at a flow rate of 300 nL/min controlled by IntelliFlow technology. The mass spectrometer was operated in the positive ion mode. MS data were acquired using a data-dependent top10 method that dynamically selected the most abundant precursor ions from the survey scan (300–1800 m/z) for HCD fragmentation. The automatic gain control (AGC) target was set to 1e6, and the maximum inject time was set to 50 ms. The dynamic exclusion duration was 60.0 s. Survey scans were acquired at a resolution of 70,000 at 200 m/z , the resolution for HCD spectra was set to 17,500 at 200 m/z , and the isolation window was 2 m/z . The normalized collision energy was 30 eV, and the underfill ratio was defined as 0.1%. The instrument was run with the peptide recognition mode enabled.

2.18.5. Data processing

All data were analyzed using MaxQuant software version 1.5.3.17. Proteins were identified by comparing all the spectra with the human proteome reference database (Swissprot_human_20422_20,190,522.fasta). Enzymatic digestion was performed using trypsin, and the maximum number of missed cleavages allowed was two. In addition, the oxidation of methionine was selected as a variable modification, while the carbamidomethylation of cysteine was selected as a fixed modification. Razor and unique peptides were used for protein quantification. In the MS mode, an initial mass tolerance of 6 ppm was selected, and the MS/MS tolerance was set to 20 ppm for fragmentation data. The false discovery rate (FDR) was specified as 0.01 for proteins and peptides. Intensity-based absolute quantification (iBAQ) was performed using the default parameters in MaxQuant.

2.18.6. Bioinformatics analysis

The identified iMSC-IEVs proteins were compared with the results from the Vesiclepedia database using FunRich Software (Version 3.1.3). The gene ontology (GO) enrichment analysis was also processed by FunRich Software (Version 3.1.3). Canonical pathway analysis was performed using the Ingenuity Pathway Analysis (IPA, Qiagen).

2.19. Statistical analysis

GraphPad Prism 8 Software (CA, USA) was utilized for statistical analysis in this study. The Student's *t*-test was performed for comparison between two groups. One-way ANOVA was employed for comparison among various groups. Two-way ANOVA was used to measure the differences across three or more groups over time. Besides, two-tailed Pearson correlation analyses were adopted for linear regression analysis. Statistical significance was set as $P < 0.05$. All data were presented as mean \pm standard deviation (S.D.).

3. Results

3.1. Isolation and characterization of iMSC-sEVs and iMSC-IEVs

In this study, iPSC-derived MSCs (iMSCs) were adopted as producing sources for the sEVs and IEVs. We have successfully generated iMSCs according to our previous reports [27,32]. Flow cytometer analysis showed that iMSCs expressed specific surface markers (Fig. S1).

iMSC-sEVs (sEVs) and iMSC-IEVs (IEVs) were isolated and collected from the iMSCs culture medium using differential centrifugation (Fig. 1a). The isolated iMSC-sEVs displayed a size around 100 nm while iMSC-IEVs displayed a size above 200 nm, both of them exhibited a cup-shaped morphology as shown by TEM (Fig. 1b). Western blot analysis showed that both sEVs and IEVs highly expressed CD9, CD63, and TSG 101, but were negative for the Golgi-related protein GM130 (Fig. 1c). NTA revealed that the size distribution of most sEVs was below 200 nm and displayed a peak diameter at 105 nm, while the size distribution of IEVs varied from 0 to 600 nm and displayed a peak diameter at 225 nm (Fig. 1d and e). Additionally, the yields of sEVs and IEVs were calculated in accordance with particle concentration and protein concentration. The mean particle concentration of sEVs was $12.00 \times 10^7 \pm 1.26 \times 10^7$ particles per mL in the culture medium (CM) and 1440.00 ± 151.04 particles per cell, while the mean particle concentration of IEVs was $2.16 \times 10^7 \pm 0.10 \times 10^7$ particles per mL in the culture medium (CM) and 259.60 ± 12.45 particles per cell. Besides, the mean protein concentration of sEVs was 4661.17 ± 80.09 ng per mL in CM and $3.92 \times 10^{-5} \pm 0.37 \times 10^{-5}$ ng per particle, while the mean protein concentration of IEVs was 3883.00 ± 66.15 ng per mL in CM and $18.00 \times 10^{-5} \pm 1.08 \times 10^{-5}$ ng per particle (Fig. 1f).

3.2. iMSC-IEVs alleviate tendinopathy-related pain and reduce inflammation in vivo

As pain was characterized as one of the major concerns of tendinopathy, we first established a rat tendinopathy model and assessed the analgesic effect of iMSC-IEVs *in vivo*. A dose of 100 μL IEVs (10^9 particles/mL) were adopted to treat tendinopathy rats weekly as described above, while a dose of 100 μL sEVs (10^{10} particles/mL) was conducted as a comparative therapy at the same time point. The dose used for IEVs and sEVs treatment were determined according to their yields from the same volume of supernatant in Fig. 1f. The local injection of IEVs or sEVs was performed under ultrasonic guidance in order to inject EVs into the peri-tendon space of quadriceps tendon (Figs. S2a–b). The peri-tendon retention of IEVs or sEVs were visualized by an IVIS Spectrum imaging system at different time points (2 h, 24 h, and 48 h) after injection (Fig. S2c). Results of static pain-related behaviors analyses including hind-paw withdrawal threshold (PWT) and static weight-bearing (SWB) indicated that IEVs application relieved pain of the rat with tendinopathy following 4 weeks of treatment (Fig. 2a). Then gait analysis was used to evaluate the dynamic pain-related behaviors at 4 weeks after treatment. Print area, swing speed, and duty cycle analyses indicated that IEVs administration significantly improved the dynamic walking pattern of tendinopathy rats compared with PBS group (Fig. 2b and c). Importantly, the results of above pain-related behaviors revealed that IEVs treatment possessed similar analgesic function as sEVs. Next, Hematoxylin-Eosin (HE) staining was performed to evaluate the tendon abnormalities after 4 weeks treatment. Semi-quantitative histological analysis showed that the Bonar score (assessed by cell morphology, cellularity, and vascularity indexes) was significantly lower in the IEVs group than the PBS group, indicating IEVs facilitated tendon repair in tendinopathy (Fig. 2d and e). Since macrophages play a crucial role in inflammatory process and tissue healing in the pathogenesis of tendinopathy [6], we therefore investigated the effect of IEVs on macrophage phenotypes infiltration. The immunofluorescent staining showed that DiI-labeled sEVs/IEVs were mainly internalized by CD68⁺ macrophages at 24 h after injection, while less sEVs/IEVs were internalized by SCX⁺ tenocytes and CD146⁺ tendon stem/progenitor cells (Fig. S3). The results of immunohistochemical (IHC) staining showed that IEVs treatment reduced the infiltration of CD86⁺ M1 macrophages while promoted the infiltration of CD206⁺ M2 macrophages at 2 weeks and 4 weeks after treatment (Fig. 2d and e), and IEVs group showed no significant differences to the sEVs group, suggesting they had similar capacity in regulating macrophage infiltration. The correlation analysis between the macrophage phenotypes and the pain-related indexes

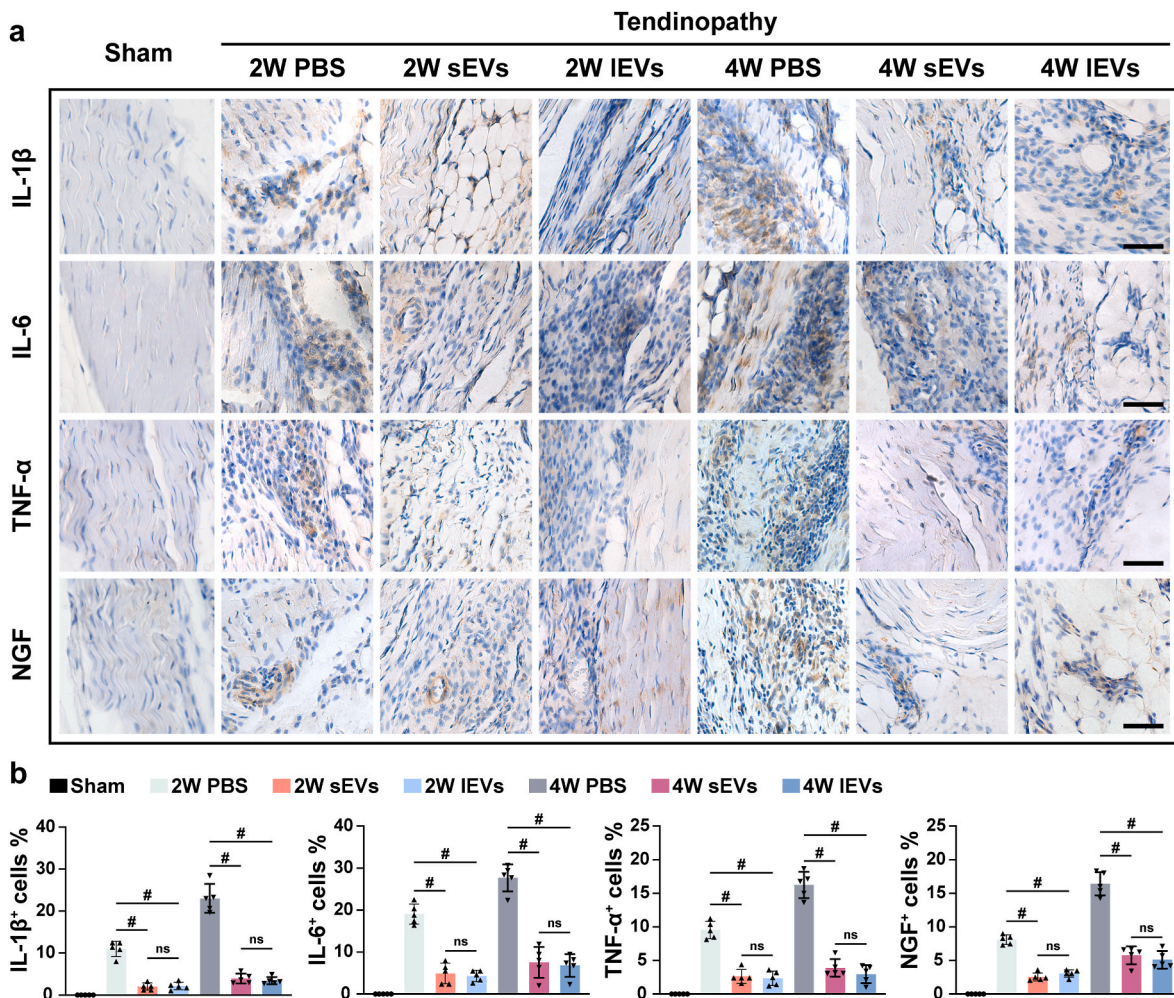


Fig. 3. iMSC-IEVs treatment reduced the expression of inflammatory cytokines *in vivo*. (a) Representative images of HE staining and immunohistochemical staining for IL-1 β , IL-6, TNF- α , and NGF in each group. Scale bar: 100 μ m. (b) Quantitative analysis of immunohistochemical staining for IL-1 β , IL-6, TNF- α , and NGF in each group (n = 5/group). * P < 0.05, ** P < 0.01, *** P < 0.001, # P < 0.0001, ns, nonsignificant difference.

(including PWT, SWB, print area, swing speed, and duty cycle) at 4 weeks after treatment showed that the pain-related indexes were negatively correlated with M1 phenotype macrophages infiltration (Figs. S4a–e), but positively correlated with M2 phenotype macrophages infiltration (Figs. S4f–j), suggesting that M1 macrophage infiltration could exacerbate the tendinopathy-related pain, while M2 macrophage infiltration could ameliorate the tendinopathy-related pain.

Specifically, pro-inflammatory cytokines are regarded as important mediators of pain [33]. We then checked the expression of several pro-inflammatory cytokines including IL-1 β , TNF α , IL-6, and NGF in each group. The IHC staining showed that both IEVs and sEVs treatment markedly reduced the expression of those pro-inflammatory factors at 2 weeks and 4 weeks after treatment (Fig. 3a and b). Collectively, these data demonstrated that IEVs treatment possessed anti-inflammatory function and analgesic effect in the rat tendinopathy model, similar to the capacity of sEVs.

3.3. iMSC-IEVs regulate M1 macrophages towards M2 macrophages *in vitro*

To further investigate the regulatory effects of iMSC-IEVs on macrophage repolarization, a widely used murine macrophage cell line RAW 264.7 was adopted in this study. To determine whether IEVs as well as sEVs could be internalized by RAW 264.7 cells, DiI fluorescent dye labeled IEVs and sEVs were added to culture medium RAW 264.7

cells for 6 h. The results showed that RAW264.7 cells could uptake both of them at 37 $^{\circ}$ C incubation but not 4 $^{\circ}$ C incubation (Fig. S5). Next, RAW 264.7 cells were stimulated with 100 ng/ml lipopolysaccharide (LPS) for 6 h to induce M1 phenotype macrophages and followed by vehicle, sEVs or IEVs treatment for 48 h. Cells without LPS stimulation and following treatment were regarded as M0 phenotype macrophages. Based on the RT-qPCR analysis, IEVs treatment decreased the expression of pro-inflammatory genes (Fig. 4a–e), and increased the expression of anti-inflammatory genes (Fig. 4f–i) in a dose-dependent manner. Consistently, flow cytometry analysis revealed that the percentage of CD86 positive cells (M1 macrophages) decreased while the percentage of CD206 positive cells (M2 macrophages) increased following IEVs treatment in a dose-dependent manner (Fig. 4j and k). Specifically, 10⁸ particles/mL IEVs could fulfill similar function as 10⁹ particles/mL sEVs. Therefore, 10⁸ particles/mL IEVs and 10⁹ particles/mL sEVs were used for the following experiments. Moreover, immunofluorescence staining was conducted for the M1 macrophage and M2 macrophage markers, which showed that 10⁸ particles/mL IEVs suppressed the CD86 positive cells and promoted the CD206 positive cells as 10⁹ particles/mL sEVs (Fig. 4l–m). While LPS stimulation induced robust production of IL-1 β , TNF α , and IL-6 in the supernatant, 10⁸ particles/mL IEVs significantly reduced the levels of these pro-inflammatory cytokines as 10⁹ particles/mL sEVs and increased the levels of anti-inflammatory mediators including IL-10 and TGF β (Figure 4n). Taken together, these results suggested that iMSC-IEVs successfully repolarized M1 macrophages to

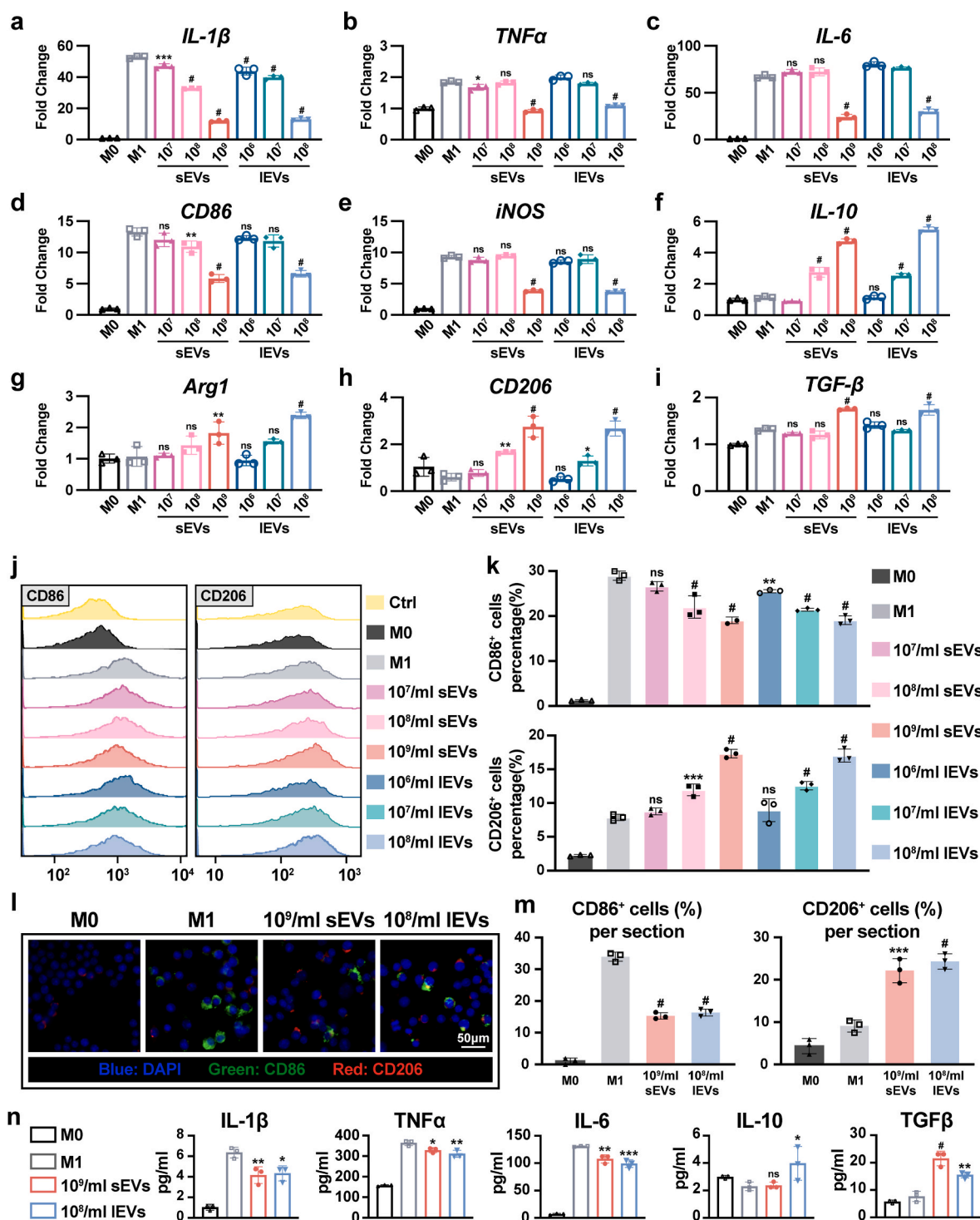


Fig. 4. iMSC-IEVs modulated macrophage polarization in a dose-dependent manner *in vitro*. (a–e) RT-qPCR analysis of pro-inflammatory genes expression in RAW 264.7 cells under different concentration of sEVs and IEVs treatment (particles/ml, n = 3/group). (f–i) RT-qPCR analysis of anti-inflammatory genes expression in RAW 264.7 cells under different concentration of sEVs and IEVs treatment (particles/ml, n = 3/group). (j) Flow cytometry analysis of the M1 macrophage marker (CD86) and M2 macrophage marker (CD206) in RAW 264.7 cells. (k) Quantitative analysis of the CD86⁺ macrophage percentage and CD206⁺ macrophage percentage in flow cytometry (n = 3/group). (l) Representative images of immunofluorescence staining of CD86 and CD206 in RAW 264.7 cells. Scale bar: 50 μm. (m) Quantitative analysis of the CD86⁺ macrophage percentage and CD206⁺ macrophage percentage in immunofluorescence staining (n = 3/group). (n) Concentration of pro-inflammatory and anti-inflammatory cytokines in the supernatant of RAW 264.7 cells (n = 3/group). *P < 0.05, **P < 0.01, ***P < 0.001, #P < 0.0001, ns, nonsignificant difference vs. the M1 group.

the M2 macrophages and could inhibit inflammation.

3.4. iMSC-IEVs regulate macrophage polarization partly by mediating the p38 MAPK signaling pathway

Next, to clarify the mechanism by which iMSC-IEVs regulated

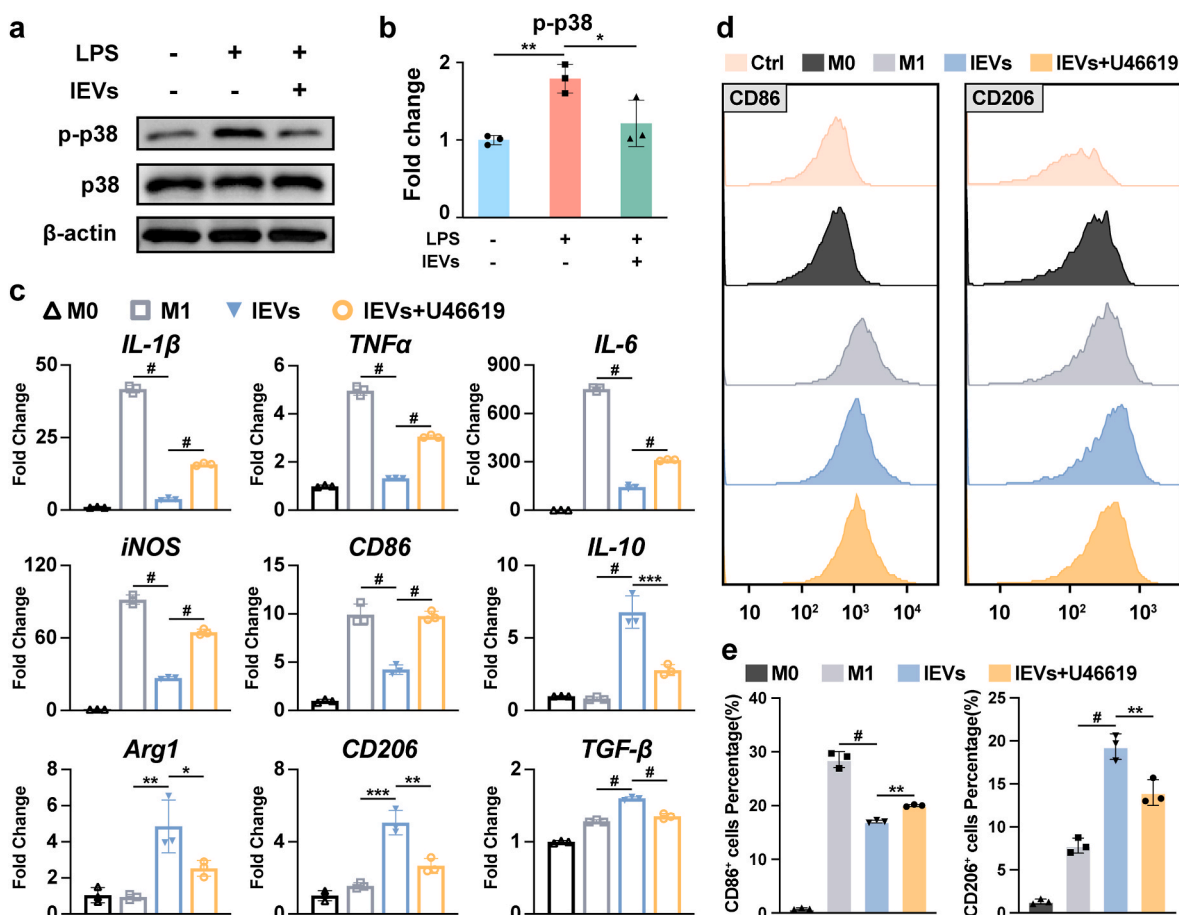


Fig. 6. iMSC-IEVs modulated macrophage polarization via mediating the p38 MAPK signaling pathway. (a–b) Western blot analysis of p-p38 and p38 expression in RAW 264.7 cells under different treatments ($n = 3/\text{group}$). (c) RT-qPCR analysis of pro-inflammatory genes and anti-inflammatory genes expression in RAW 264.7 cells under different treatments ($n = 3/\text{group}$). (d–e) Flow cytometry analysis and quantification of CD86⁺ macrophage percentage and CD206⁺ macrophage percentage under different treatments ($n = 3/\text{group}$). * $P < 0.05$, ** $P < 0.01$, *** $P < 0.001$, # $P < 0.0001$, ns, nonsignificant difference.

LPS-stimulated RAW 264.7 cells for 48 h. RT-qPCR analysis showed that the expression of pro-inflammatory genes (IL-1 β , TNF- α , IL-6, iNOS, CD86) was partly enhanced once the p38 MAPK signaling pathway was activated in the IEVs with the U-46619 group, whereas the anti-inflammatory genes expression (IL-10, Arg1, CD206, TGF- β) was partly decreased (Fig. 6c). Additionally, flow cytometry analysis was conducted to examine the M1 and M2 markers in each group. The results showed that the percentage of M1 macrophages were increased in the IEVs with U-46619 group and the percentage of M2 macrophages were lower in the IEVs with U-46619 group when compared to the IEVs group, indicating the repolarization modulating function of IEVs was partly blocked by the activation of p38 MAPK signaling pathway (Fig. 6d and e). Taken together, these results suggested that the macrophage repolarization was, at least partly, mediated by the inhibition of the p38 MAPK signaling pathway by iMSC-IEVs.

3.5. Proteomics analysis of iMSC-IEVs

Previous studies have illustrated that EVs could regulate the biological processes of recipient cells via the delivery of encapsulated proteins [31,40,41]. Herein, we performed LC-MS/MS analysis and identified a total of 2208 proteins in iMSC-IEVs. Among these identified proteins, 2074 proteins could be matched to the Vesiclepedia database whereas 134 proteins were not included in current database (Fig. 7a). The list for the 134 new-found proteins was showed in Supplemental Table 2. Subsequently, Gene Ontology (GO) analyses of cellular component, molecular function, and biological process for iMSC-IEVs

were conducted by FunRich Software (Fig. 7b–d). Cellular component analysis showed that 59.7% of the identified proteins were derived from cytoplasm (Fig. 7b). Molecular function analysis revealed that “Catalytic activity” (6.9%) was a major component for the protein category of iMSC-IEVs (Fig. 7c). Biological process analysis suggested an enrichment of proteins involved in “Metabolism” (19.2%), “Energy pathways” (18.8%), “Protein metabolism” (15.8%), “Cell growth and/or maintenance” (13.1%) etc. (Fig. 7d).

3.6. iMSC-IEVs could deliver DUSP2 and DUSP3 to macrophages

Next, we utilized IPA to analyze the potential canonical pathways in which identified iMSC-IEVs proteins were involved. The result showed that these proteins were related to a series of signaling pathways including “EIF2 signaling”, “Actin Cytoskeleton signaling”, “Sirtuin signaling”, “Integrin signaling”, “mTOR signaling”, and others (Fig. 7e). Among these signaling pathways, “EIF2 signaling”, “Integrin signaling”, “mTOR signaling”, “RHOA signaling”, “ERK/MAPK signaling”, and “HIF1 α signaling” were related to the regulation of inflammatory response. To elucidate the underlying mechanism for iMSC-IEVs-afforded regulatory function of p38 MAPK signaling pathway, we examined the catalogue of “ERK/MAPK signaling” combining with p38 MAPK signaling pathway in KEGG database, and found DUSP2 (also known as PAC1) and DUSP3, which were responsible for the p38 dephosphorylation [42,43], were enriched in iMSC-IEVs. The expression of DUSP2 and DUSP3 in iMSC and iMSC-IEVs were validated by Western blot analysis (Fig. 7f). To verify iMSC-IEVs could transport these two

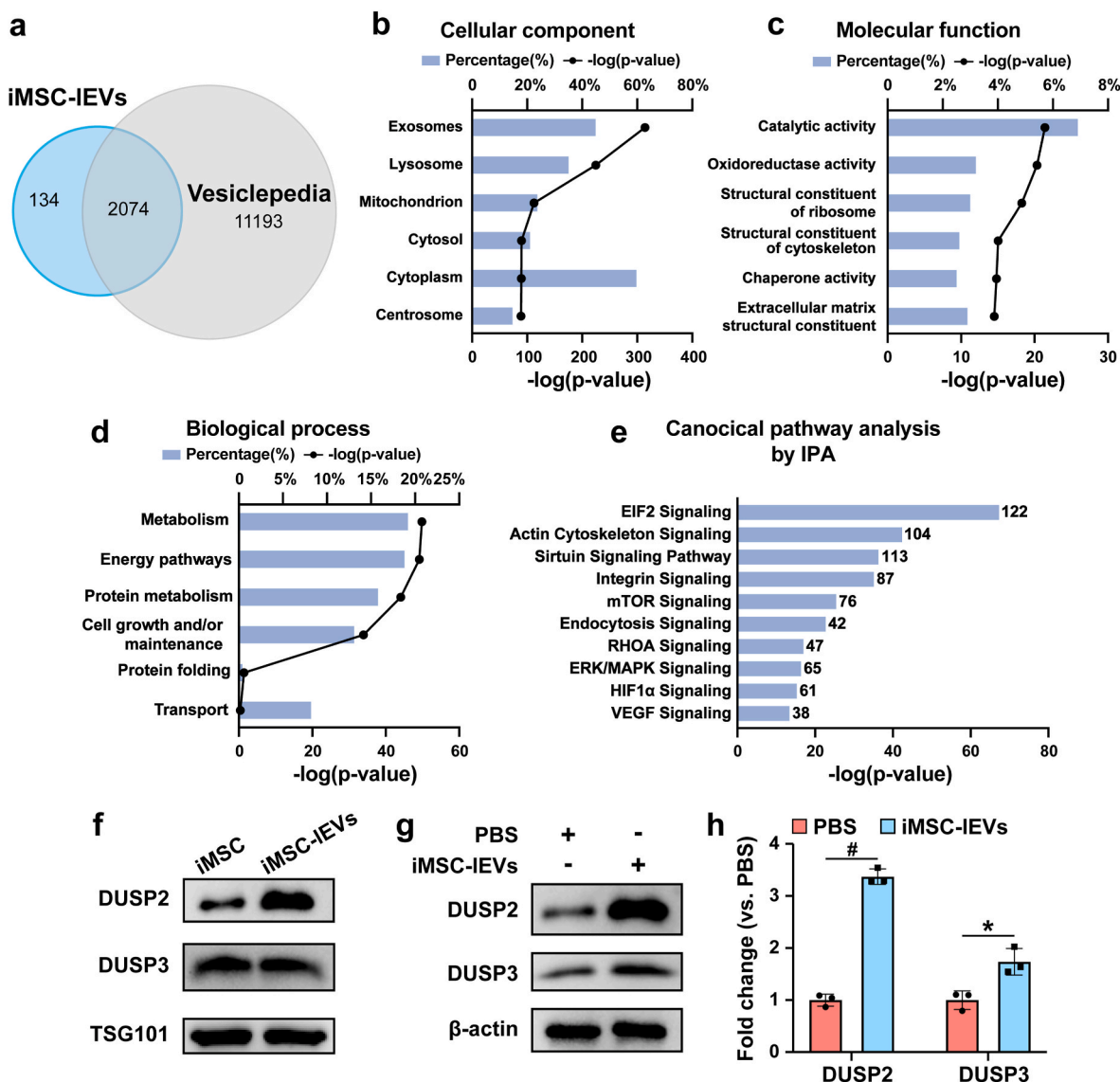


Fig. 7. Proteomics analysis of iMSC-IEVs. (a) Venn diagram showing the overlapping and unique proteins in iMSC-IEVs with Vesiclepedia database. (b) Gene Ontology Cellular Component analysis of proteins enriched in iMSC-IEVs. (c) Gene Ontology Molecular Function analysis of proteins enriched in iMSC-IEVs. (d) Gene Ontology Biological Process analysis of proteins enriched in iMSC-IEVs. (e) IPA displaying canonical pathway analysis of iMSC-IEVs proteins. (f) Representative bands of DUSP2, DUSP3, and TSG101 in iMSCs and iMSC-IEVs by Western blot analysis. (g–h) Western blot analysis of DUSP2 and DUSP3 in macrophages under different treatments ($n = 3/\text{group}$). * $P < 0.05$, ** $P < 0.01$, *** $P < 0.001$, # $P < 0.0001$, ns, nonsignificant difference.

proteins to recipient cells, macrophages were incubated with iMSC-IEVs. Western blot analysis showed that the expressions of DUSP2 and DUSP3 in M1 macrophages were both increased after the iMSC-IEVs incubation (Fig. 7g and h). Moreover, to further validate whether human derived DUSP2 and DUSP3 in iMSC-IEVs could be detected in murine RAW 264.7 macrophages after treatment, we adopted antibodies that could only recognize DUSP2 and DUSP3 from human source. The result was presented in Fig. S6 and showed that human derived DUSP2 and DUSP3 could be successfully detected in RAW 264.7 cells after iMSC-IEVs treatment. These data indicated that iMSC-IEVs could deliver the encapsulated DUSP2 and DUSP3 to the macrophages, and thereby modulating p38 signaling pathway.

3.7. iMSC-IEVs regulate the macrophage heterogeneity and infiltrated inflammatory cytokines in human tendon tissues

Since iMSC-IEVs exhibited good performance in the animal model of tendinopathy, we wondered whether iMSC-IEVs will also be effective in

patients. Therefore, tendon tissues from tendinopathy patients were obtained and incubated with iMSC-IEVs *in vitro*. The results showed that iMSC-IEVs significantly decreased the percentage of CD86⁺ M1 macrophages while increased the percentage of CD206⁺ M2 macrophages (Fig. 8a and b). Additionally, the expressions of inflammatory cytokines, including IL-1 β , TNF α , IL-6, and NGF, were reduced by the iMSC-IEVs (Fig. 8c and d). Collectively, these data were consistent with the results of our animal experiments and further confirmed the effectiveness of iMSC-IEVs on human tendon tissues, suggesting that iMSC-IEVs might be a promising therapeutic reagent for tendinopathy.

4. Discussion

Previous studies have defined tendinopathy as a “non-inflammatory” disease [44]. However, recent evidence have demonstrated the presence of immune cells and inflammatory mediators in the pathologic tendons [3,6,45]. Macrophages are considered as the major subset of immune-cytes that infiltrate to the pathologic tendons and could regulate local

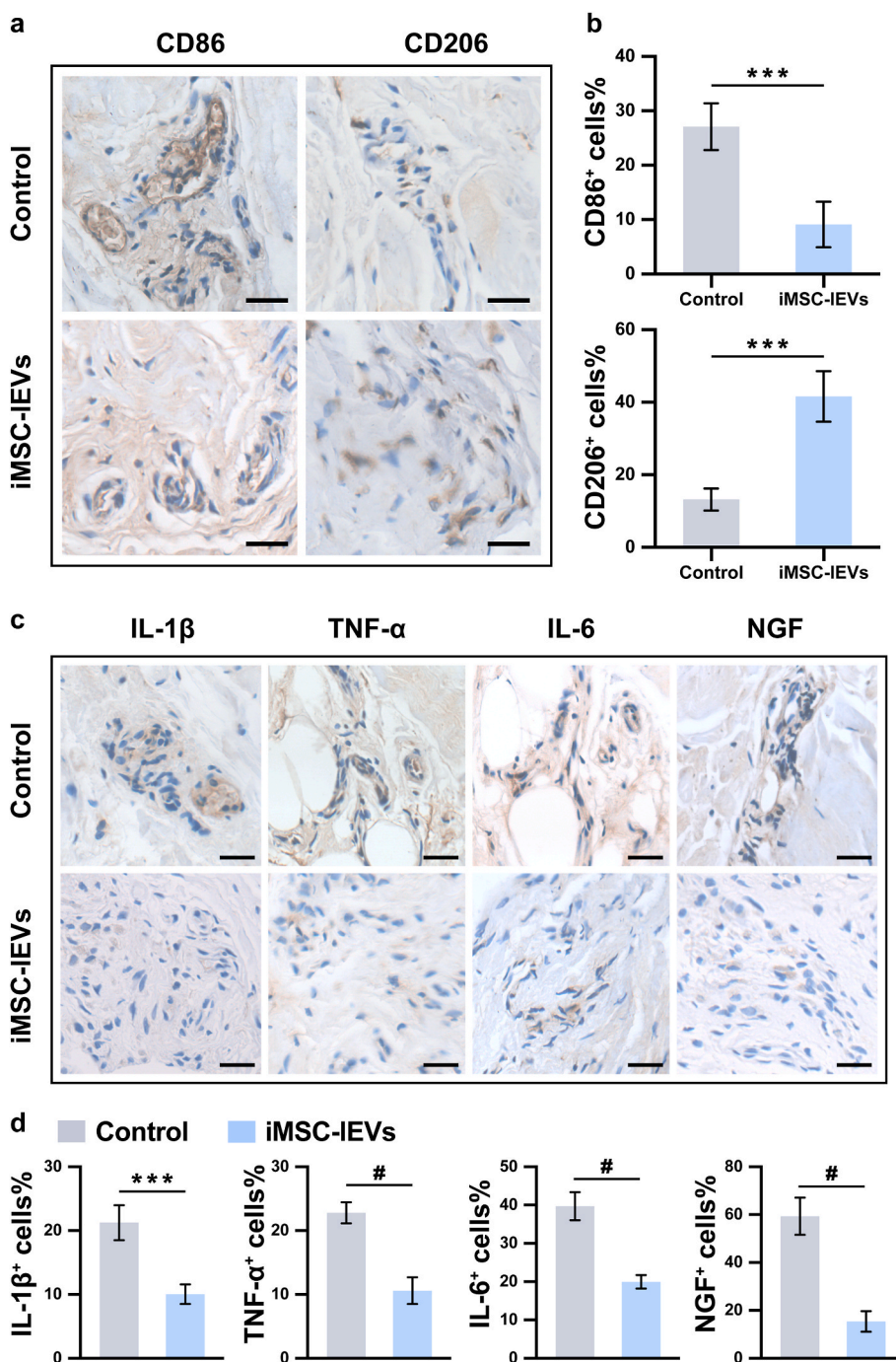


Fig. 8. iMSC-IEVs treatment regulated macrophage heterogeneity and inflammatory cytokines infiltration in human tendon tissue. (a) Representative images of immunohistochemistry staining for CD86 and CD206 expression in human tendon tissue. Scale bar: 100 μm. (b) Quantitative analysis of immunohistochemical staining for CD86 and CD206 expression in human tendon tissue. (c) Representative images of immunohistochemistry staining for IL-1β, TNF-α, IL-6, and NGF expression in human tendon tissue. Scale bar: 100 μm. (d) Quantitative analysis of immunohistochemical staining for IL-1β, TNF-α, IL-6, and NGF in human tendon tissue. **P* < 0.05, ***P* < 0.01, ****P* < 0.001, #*P* < 0.0001.

inflammation by shifting from M1 pro-inflammatory macrophages to M2 anti-inflammatory macrophages, thereby releasing different sets of cytokines [6,46]. In this study, we found that iMSC-IEVs could decrease the amount of M1 macrophages while increase the amount of M2 macrophages in both rat and human tendon tissues. Then, we further demonstrated that iMSC-IEVs could repolarize the M1 macrophages towards M2 macrophages. These data show for the first time that iMSC-IEVs possess the anti-inflammatory ability in tendinopathy by regulating the macrophage heterogeneity.

Among various symptoms of tendinopathy, pain is the most prominent and disturbing one, which can negatively influence the mental health, life quality as well as social participation of the patients [47,48]. During tendinopathy, the inflammatory mediators play as a vital role in evoking pain via direct or indirect activation and sensitization of

nociceptors [49]. Thus, the key to prevent tendinopathy-related pain is to control the inflammatory microenvironment during the progression of tendinopathy. In the present study, we found that iMSC-IEVs were efficient for improving pain-related behaviors in tendinopathy rats. Further immunohistochemical analysis revealed that iMSC-IEVs could reduce the expression of inflammatory markers (IL-1β, TNFα, IL-6, NGF) in rat tendon tissues. These data demonstrated that iMSC-IEVs were effective for ameliorating pain in tendinopathy, and this was closely correlated with the amelioration of inflammatory microenvironment. More importantly, few studies have evaluated the therapeutic function of extracellular vesicles for human tendinopathy. Our study demonstrated that iMSC-IEVs were efficient for regulating resident macrophage heterogeneity and reducing inflammation in tendons from tendinopathy patients. We provide first-hand evidence that iMSC-IEVs might be of

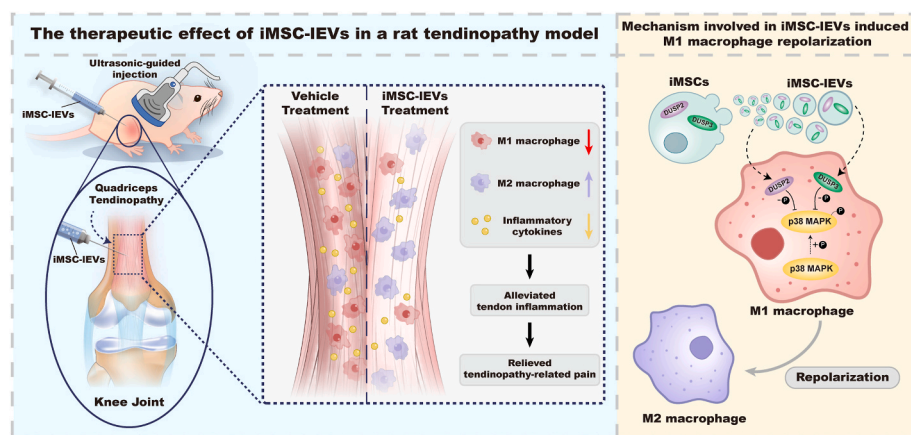


Fig. 9. Schematic illustration of the mechanisms for the therapeutic effect of iMSC-IEVs in the *in vivo* tendinopathy model as well as the regulation of macrophage repolarization. The administration of iMSC-IEVs modulated the infiltration of M1/M2 macrophages and inflammatory cytokines, and subsequently ameliorated tendinopathy-related pain *in vivo*. The p38 MAPK signaling pathway-mediated macrophage repolarization was partly regulated by the delivery of DUSP2 and DUSP3 from iMSC-IEVs.

great value in treating tendinopathy-related pain and this warrants further clinical trials.

EVs have been reported to encapsulate diverse bioactive components including RNAs, lipids, and proteins from the parental cell, which contribute to the cell-to-cell communications and regulate cell behaviors [12,13]. To the best of our knowledge, the proteins enriched in iMSC-IEVs have never been elucidated before. In this study, we performed LC-MS/MS analysis to clarify the categories of proteins in iMSC-IEVs. Totally, we identified 2208 proteins, which were highly correlated in the metabolism, energy pathway, and protein metabolism, implying the crucial role of iMSC-IEVs in regulating inflammatory and metabolic processes. Interestingly, we found a brand new set of 134 proteins that was not included in current Vesiclepedia database (detailed in Supplemental Table 2), which might be due to our in-depth quantification using fraction-based label-free proteomics analysis. Among these new-found proteins, the high-abundant ones, such as SYNPO2L, TNNT2, SEPTIN2, SEPTIN7, and SEPTIN11, were correlated with cytoskeleton formation and actin-binding activity according to previous reports [50–52], suggesting that iMSC-IEVs might also be used for those actin related diseases.

Though our data suggest that the regulatory effect by iMSC-IEVs is mediated by p38 MAPK signaling pathway, we do not rule out the potential participations of other pathways. Indeed, IPA analysis showed that the identified proteins were involved in various canonical pathways, which might have protean effects in a synergistic manner. Therefore, further studies are still required for digging out the underlying mechanisms for the immunomodulatory functions of iMSC-IEVs.

Another concern of our study was to investigate the comparative yields and therapeutic effect of sEVs and IEVs isolated from the same volume of iMSCs culture medium. In recent years, a few studies have examined and compared the functional differences between sEVs and IEVs while the conclusions were controversial. Cosenza et al. reported that sEVs derived from bone marrow MSCs were more efficient than IEVs in suppressing inflammation [53]. Saludas et al. found no differences in the anti-fibrotic capacity between sEVs and IEVs derived from cardiac progenitor cells [54]. In this study, the NTA size distribution analysis, TEM, and Western analysis revealed the successful separation of sEVs and IEVs. According to our quantification parameters of sEVs and IEVs, the yield of IEVs per mL culture medium was about 6-times lower than sEVs, which means about 4×10^9 particles IEVs and 2.4×10^{10} particles sEVs could be isolated from 200 mL culture medium using differential centrifugation combined with ultracentrifugation. Interestingly, we further found that 1×10^9 particles/mL IEVs could achieve similar functions as 1×10^{10} particles/mL sEVs both *in vivo* and *in vitro*, suggesting that single particle of IEVs might encapsulate more profitable molecules (such as nucleic acids, lipids, and proteins) due to their larger size. Taken together, our study demonstrated similar therapeutic functions between iMSC-IEVs and iMSC-sEVs, implying that there is no need

for removing large EVs during the sEVs isolation procedure when the EVs products were utilized for treating inflammatory diseases.

In summary, we demonstrated that iMSC-IEVs alleviate pain and attenuate inflammation in tendinopathy *via* polarizing the inflammatory macrophages towards the anti-inflammatory macrophages partly through mediating p38 MAPK signaling pathway by the delivery of DUSP2 and DUSP3 (Fig. 9). These findings revealed the specific role of iMSC-IEVs in immune modulation and highlighted a novel efficient cell-free therapy for the improvement of tendinopathy as well as other inflammatory diseases.

Ethics approval and consent to participate

All animal experimental procedures were approved by the Animal Research Committee of Shanghai Jiao Tong University Affiliated Sixth People's Hospital (SYXK2021-0028, Shanghai, China). The Ethics approval for the acquisition of human iliopsoas tendons was obtained from the Shanghai Sixth People's Hospital Ethics Committee (Approval code: 2022-KY-084(K)).

CRediT authorship contribution statement

Teng Ye: Conceptualization, Investigation, Writing – original draft. **Zhengsheng Chen:** Investigation, Writing – original draft. **Jiyeuan Zhang:** Writing – original draft, Data curation. **Lei Luo:** Investigation. **Renzhi Gao:** Investigation. **Liangzhi Gong:** Investigation. **Yuhang Du:** Resources. **Zongping Xie:** Writing – review & editing. **Bizeng Zhao:** Funding acquisition. **Qing Li:** Conceptualization, Writing – review & editing. **Yang Wang:** Funding acquisition.

Declaration of competing interest

The authors declare no conflict of interest.

Acknowledgements

Teng Ye, Zhengsheng Chen, and Jiyeuan Zhang contributed equally to this work. This work was supported by the National Natural Science Foundation of China (Grant No. 81870972, 82072550) and the Science and Technology Commission of Shanghai Municipality (Grant No. 21DZ2201300).

Appendix A. Supplementary data

Supplementary data to this article can be found online at <https://doi.org/10.1016/j.bioactmat.2022.08.007>.

References

- [1] N.L. Millar, K.G. Silbernagel, K. Thorborg, P.D. Kirwan, L.M. Galatz, G.D. Abrams, et al., Tendinopathy. *Nat Rev Dis Primers*. 7 (1) (2021) 1.
- [2] N.L. Millar, G.A. Murrell, I.B. McInnes, Inflammatory mechanisms in tendinopathy - towards translation. *Nat. Rev. Rheumatol.* 13 (2) (2017) 110–122.
- [3] S.G. Dakin, F.O. Martinez, C. Yapp, G. Wells, U. Oppermann, B.J. Dean, et al., Inflammation activation and resolution in human tendon disease. *Sci. Transl. Med.* 7 (311) (2015) 311ra173.
- [4] S.G. Dakin, J. Dudhia, R.K. Smith, Resolving an inflammatory concept: the importance of inflammation and resolution in tendinopathy. *Vet. Immunol. Immunopathol.* 158 (3–4) (2014) 121–127.
- [5] M. Liu, A.R. Khan, J. Ji, G. Lin, X. Zhao, G. Zhai, Crosslinked self-assembled nanoparticles for chemo-sonodynamic combination therapy favoring antitumor, antimetastasis management and immune responses. *J. Contr. Release* 290 (2018) 150–164.
- [6] J.Y. Sunwoo, C.D. Eliasberg, C.B. Carballo, S.A. Rodeo, The role of the macrophage in tendinopathy and tendon healing. *J. Orthop. Res.* 38 (8) (2020) 1666–1675.
- [7] A. Sica, A. Mantovani, Macrophage plasticity and polarization: in vivo veritas. *J. Clin. Invest.* 122 (3) (2012) 787–795.
- [8] D.M. Mosser, J.P. Edwards, Exploring the full spectrum of macrophage activation. *Nat. Rev. Immunol.* 8 (12) (2008) 958–969.
- [9] M. Liu, H. Lutz, D. Zhu, K. Huang, Z. Li, P.C. Dinh, et al., Bispecific antibody inhalation therapy for redirecting stem cells from the lungs to repair heart injury. *Adv. Sci.* 8 (1) (2020), 2002127.
- [10] K.B. Sugg, J. Lubardic, J.P. Gumucio, C.L. Mendias, Changes in macrophage phenotype and induction of epithelial-to-mesenchymal transition genes following acute Achilles tenotomy and repair. *J. Orthop. Res.* 32 (7) (2014) 944–951.
- [11] V.A. Fadok, D.L. Bratton, A. Konowal, P.W. Freed, J.Y. Westcott, P.M. Henson, Macrophages that have ingested apoptotic cells in vitro inhibit proinflammatory cytokine production through autocrine/paracrine mechanisms involving TGF- β , PGE₂, and PAF. *J. Clin. Invest.* 101 (4) (1998) 890–898.
- [12] H. Valadi, K. Ekström, A. Bossios, M. Sjöstrand, J.J. Lee, J.O. Lötvall, Exosome-mediated transfer of mRNAs and microRNAs is a novel mechanism of genetic exchange between cells. *Nat. Cell Biol.* 9 (6) (2007) 654–659.
- [13] C. Théry, L. Zitvogel, S. Amigorena, Exosomes: composition, biogenesis and function. *Nat. Rev. Immunol.* 2 (8) (2002) 569–579.
- [14] C. Théry, K.W. Witwer, E. Aikawa, M.J. Alcaraz, J.D. Anderson, R. Andriantsitohaina, et al., Minimal information for studies of extracellular vesicles 2018 (MISEV2018): a position statement of the International Society for Extracellular Vesicles and update of the MISEV2014 guidelines. *J. Extracell. Vesicles* 7 (1) (2018), 1535750.
- [15] Y. Huang, B. He, L. Wang, B. Yuan, H. Shu, F. Zhang, et al., Bone marrow mesenchymal stem cell-derived exosomes promote rotator cuff tendon-bone healing by promoting angiogenesis and regulating M1 macrophages in rats. *Stem Cell Res. Ther.* 11 (1) (2020) 496.
- [16] Y. Wang, G. He, Y. Guo, H. Tang, Y. Shi, X. Bian, et al., Exosomes from tendon stem cells promote injury tendon healing through balancing synthesis and degradation of the tendon extracellular matrix. *J. Cell Mol. Med.* 23 (8) (2019) 5475–5485.
- [17] X. Wu, T. Yan, Z. Wang, X. Wu, G. Cao, C. Zhang, et al., Micro-vesicles derived from human Wharton's Jelly mesenchymal stromal cells mitigate renal ischemia-reperfusion injury in rats after cardiac death renal transplantation. *J. Cell. Biochem.* 119 (2) (2018) 1879–1888.
- [18] Q. Lei, F. Gao, T. Liu, W. Ren, L. Chen, Y. Cao, et al., Extracellular vesicles deposit PCNA to rejuvenate aged bone marrow-derived mesenchymal stem cells and slow age-related degeneration. *Sci. Transl. Med.* 13 (578) (2021).
- [19] J. Liao, Z. Wu, Y. Wang, L. Cheng, C. Cui, Y. Gao, et al., Enhanced efficiency of generating induced pluripotent stem (iPS) cells from human somatic cells by a combination of six transcription factors. *Cell Res.* 18 (5) (2008) 600–603.
- [20] X. Liu, Y. Yang, Y. Li, X. Niu, B. Zhao, Y. Wang, et al., Integration of stem cell-derived exosomes with in situ hydrogel glue as a promising tissue patch for articular cartilage regeneration. *Nanoscale* 9 (13) (2017) 4430–4438.
- [21] C. Théry, S. Amigorena, G. Raposo, A. Clayton, Isolation and characterization of exosomes from cell culture supernatants and biological fluids. *Curr Protoc Cell Biol* 30 (2006) 3.22.1–3.22.29 (Chapter 3):Unit 3.22.
- [22] S.P. Lake, H.L. Anson, L.J. Soslowsky, Animal models of tendinopathy. *Disabil. Rehabil.* 30 (20–22) (2008) 1530–1541.
- [23] S.M. Eskildsen, D.J. Berkoff, S.A. Kallianos, P.S. Weinhold, The use of an IL1-receptor antagonist to reverse the changes associated with established tendinopathy in a rat model. *Scand. J. Med. Sci. Sports* 29 (1) (2019) 82–88.
- [24] D.J. Berkoff, S.A. Kallianos, S.M. Eskildsen, P.S. Weinhold, Use of an IL1-receptor antagonist to prevent the progression of tendinopathy in a rat model. *J. Orthop. Res.* 34 (4) (2016) 616–622.
- [25] Z. Zhu, R. Gao, T. Ye, K. Feng, J. Zhang, Y. Chen, et al., The therapeutic effect of iMSC-derived small extracellular vesicles on tendinopathy related pain through alleviating inflammation: an in vivo and in vitro study. *J. Inflamm. Res.* 15 (2022) 1421–1436.
- [26] V. Deshmukh, T. Seo, A.L. O'Green, M. Ibanez, B. Hofilena, S. Kc, et al., SM04755, a small-molecule inhibitor of the Wnt pathway, as a potential topical treatment for tendinopathy. *J. Orthop. Res.* 39 (9) (2021) 2048–2061.
- [27] K. Feng, X. Xie, J. Yuan, L. Gong, Z. Zhu, J. Zhang, et al., Reversing the surface charge of MSC-derived small extracellular vesicles by ePL-PEG-DSPE for enhanced osteoarthritis treatment. *J. Extracell. Vesicles* 10 (13) (2021), e12160.
- [28] A.F. Gabriel, M.A. Marcus, W.M. Honig, G.H. Walenkamp, E.A. Joosten, The CatWalk method: a detailed analysis of behavioral changes after acute inflammatory pain in the rat. *J. Neurosci. Methods* 163 (1) (2007) 9–16.
- [29] N. Maffulli, U.G. Longo, F. Franceschi, C. Rabitti, V. Denaro, Movin and Bonar scores assess the same characteristics of tendon histology. *Clin. Orthop. Relat. Res.* 466 (7) (2008) 1605–1611.
- [30] Y. Xia, X. Ling, G. Hu, Q. Zhu, J. Zhang, Q. Li, et al., Small extracellular vesicles secreted by human iPSC-derived MSC enhance angiogenesis through inhibiting STAT3-dependent autophagy in ischemic stroke. *Stem Cell Res. Ther.* 11 (1) (2020) 313.
- [31] L. Gong, B. Chen, J. Zhang, Y. Sun, J. Yuan, X. Niu, et al., Human ESC-seV's alleviate age-related bone loss by rejuvenating senescent bone marrow-derived mesenchymal stem cells. *J. Extracell. Vesicles* 9 (1) (2020), 1800971.
- [32] Y. Yang, Z. Zhu, R. Gao, J. Yuan, J. Zhang, H. Li, et al., Controlled release of MSC-derived small extracellular vesicles by an injectable Diels-Alder crosslinked hyaluronic acid/PEG hydrogel for osteoarthritis improvement. *Acta Biomater.* 128 (2021) 163–174.
- [33] B.A.A. Al-Dhafer, H.S. Joo, S.Y. Park, Y.H. Shin, J.K. Kim, Increased expression of macrophages and inflammatory cytokines at tendon origin in patients with chronic lateral epicondylitis. *J. Shoulder Elbow Surg.* 30 (7) (2021) 1487–1493.
- [34] H. Ning, H. Chen, J. Deng, C. Xiao, M. Xu, L. Shan, et al., Exosomes secreted by FNDC5-BMMSCs protect myocardial infarction by anti-inflammation and macrophage polarization via NF- κ B signaling pathway and Nrf2/HO-1 axis. *Stem Cell Res. Ther.* 12 (1) (2021) 519.
- [35] T. Yu, M. Gao, P. Yang, D. Liu, D. Wang, F. Song, et al., Insulin promotes macrophage phenotype transition through PI3K/Akt and PPAR- γ signaling during diabetic wound healing. *J. Cell. Physiol.* 234 (4) (2019) 4217–4231.
- [36] F. Zhou, J. Mei, X. Han, H. Li, S. Yang, M. Wang, et al., Kinesinidate attenuates osteoarthritis by repolarizing macrophages through inactivating NF- κ B/MAPK signaling and protecting chondrocytes. *Acta Pharm. Sin. B* 9 (5) (2019) 973–985.
- [37] L. Liu, Y. Zhang, X. Zheng, L. Jin, N. Xiang, M. Zhang, et al., Eosinophils attenuate arthritis by inducing M2 macrophage polarization via inhibiting the I κ B/P38 MAPK signaling pathway. *Biochem. Biophys. Res. Commun.* 508 (3) (2019) 894–901.
- [38] Y.X. Wu, F.J. Jiang, G. Liu, Y.Y. Wang, Z.Q. Gao, S.H. Jin, et al., Dehydrocostus lactone attenuates methicillin-resistant *Staphylococcus aureus*-induced inflammation and acute lung injury via modulating macrophage polarization. *Int. J. Mol. Sci.* 22 (18) (2021).
- [39] L. Zhang, Q. Meng, N. Yepuri, G. Wang, X. Xi, R.N. Cooney, Surfactant proteins-A and -D attenuate LPS-induced apoptosis in primary intestinal epithelial cells (IECs). *Shock* 49 (1) (2018) 90–98.
- [40] J.S. Choi, W.L. Cho, Y.J. Choi, J.D. Kim, H.A. Park, S.Y. Kim, et al., Functional recovery in photo-damaged human dermal fibroblasts by human adipose-derived stem cell extracellular vesicles. *J. Extracell. Vesicles* 8 (1) (2019), 1565885.
- [41] R. Upadhyay, L.N. Madhu, S. Attaluri, D.L.G. Gitai, M.R. Pinson, M. Kodali, et al., Extracellular vesicles from human iPSC-derived neural stem cells: miRNA and protein signatures, and anti-inflammatory and neurogenic properties. *J. Extracell. Vesicles* 9 (1) (2020), 1809064.
- [42] W. Wei, Y. Jiao, A. Postlethwaite, J.M. Stuart, Y. Wang, D. Sun, et al., Dual-specificity phosphatases 2: surprising positive effect at the molecular level and a potential biomarker of diseases. *Gene Immun.* 14 (1) (2013) 1–6.
- [43] L.F. Monteiro, P.Y.M. Ferruzo, L.C. Russo, J.O. Farias, F.L. Forti, DUSP3/VHR: a druggable dual phosphatase for human diseases. *Rev. Physiol. Biochem. Pharmacol.* 176 (2019) 1–35.
- [44] M. Abate, K.G. Silbernagel, C. Siljeholm, A. Di Iorio, D. De Amicis, V. Salini, et al., Pathogenesis of tendinopathies: inflammation or degeneration? *Arthritis Res. Ther.* 11 (3) (2009) 235.
- [45] B.J. Dean, S.J. Snelling, S.G. Dakin, R.J. Murphy, M.K. Javaid, A.J. Carr, Differences in glutamate receptors and inflammatory cell numbers are associated with the resolution of pain in human rotator cuff tendinopathy. *Arthritis Res. Ther.* 17 (1) (2015) 176.
- [46] T.A. Wynn, K.M. Vannella, Macrophages in tissue repair, regeneration, and fibrosis. *Immunity* 44 (3) (2016) 450–462.
- [47] A.M. Fearon, J.L. Cook, J.M. Scarvell, T. Neeman, W. Cormick, P.N. Smith, Greater trochanteric pain syndrome negatively affects work, physical activity and quality of life: a case control study. *J. Arthroplasty* 29 (2) (2014) 383–386.
- [48] H.S. Picavet, N. Hoeymans, Health related quality of life in multiple musculoskeletal diseases: SF-36 and EQ-5D in the DMC3 study. *Ann. Rheum. Dis.* 63 (6) (2004) 723–729.
- [49] D. Julius, A.I. Basbaum, Molecular mechanisms of nociception. *Nature* 413 (6852) (2001) 203–210.
- [50] P. Gaudet, M.S. Livstone, S.E. Lewis, P.D. Thomas, Phylogenetic-based propagation of functional annotations within the Gene Ontology consortium. *Briefings Bioinf.* 12 (5) (2011) 449–462.
- [51] L. Thierfelder, H. Watkins, C. MacRae, R. Lamas, W. McKenna, H.P. Vosberg, et al., Alpha-tropomyosin and cardiac troponin T mutations cause familial hypertrophic cardiomyopathy: a disease of the sarcomere. *Cell* 77 (5) (1994) 701–712.
- [52] M. Sirajuddin, M. Farkasovsky, F. Hauer, D. Kühlmann, I.G. Macara, M. Weyand, et al., Structural insight into filament formation by mammalian septins. *Nature* 449 (7160) (2007) 311–315.
- [53] S. Cosenza, K. Toupet, M. Maumus, P. Luz-Crawford, O. Blanc-Brude, C. Jorgensen, et al., Mesenchymal stem cells-derived exosomes are more immunosuppressive than microparticles in inflammatory arthritis. *Theranostics* 8 (5) (2018) 1399–1410.
- [54] L. Saludas, E. Garbayo, A. Ruiz-Villalba, S. Hernández, P. Vader, F. Prósper, et al., Isolation methods of large and small extracellular vesicles derived from cardiovascular progenitors: a comparative study. *Eur. J. Pharm. Biopharm.* 170 (2021) 187–196.